Materials and Design 195 (2020) 109064

Contents lists available at ScienceDirect

Materials and Design

journal homepage: www.elsevier.com/locate/matdes

Boride formation behaviour and their effect on tensile ductility in cast TiAl-based alloys

Jing Li [a,*], Spencer Jeffs [a], Mark Whittaker [a], Nigel Martin [b]

[a] Institute of Structural Materials, College of Engineering, Swansea University, Swansea SA1 8EN, UK
[b] Rolls-Royce Plc, P.O. Box 31, Derby DE24 8BJ, UK

HIGHLIGHTS

- Hf promotes the formation of thin curvy boride flakes whilst Ta promotes the formation of thick straight boride ribbons.
- Coarse long boride has TiB(B27) crystal structure and curvy flake boride has TiB(B_f) crystal structure.
- Curvy borides have the strongest effect in reducing ductility, regardless of alloy composition.

GRAPHICAL ABSTRACT

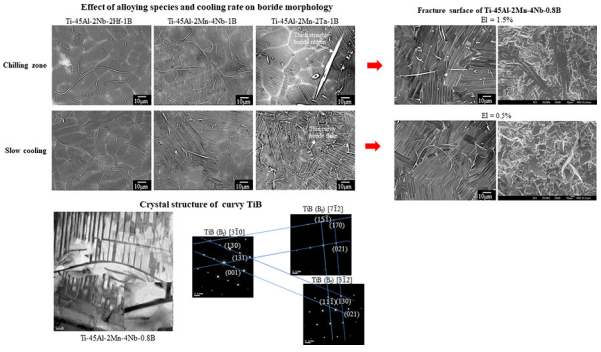

ARTICLE INFO

Article history:
Received 25 April 2020
Received in revised form 15 July 2020
Accepted 14 August 2020
Available online 18 August 2020

Keywords:
Titanium aluminides
Borides
Microstructure
Mechanical properties

ABSTRACT

Boron has been used to refine the microstructures in TiAl castings, such as low-pressure turbine (LPT) blades, to improve mechanical properties. However, boride precipitates with undesirable morphologies could reduce ductility and even entirely remove the benefits of grain refinement. Boride size and morphology in variant alloys based on Ti45Al2Mn2Nb1B has found to be closely related to alloying element species and solidification conditions, leading to distinctly different boride formation behaviour. It has been shown that Hf promotes the formation of thin curvy boride flakes whilst Ta promotes the formation of thick straight boride ribbons in the studied cooling rate range. The boride crystal structure changes from TiB with the B27 structure for coarse straight boride to TiB with B_f structure for the curvy boride. Curvy borides have the strongest effect in reducing ductility, regardless of alloy composition.

1. Introduction

Intermetallic γ-TiAl based alloys are emerging as a potential substitution for the heavier Ni-based superalloys used in aero-engine blades, owing to their attractive high-temperature properties and low density [1–3]. The successful insertion in the GEnx and PW1000G engines that used titanium aluminides for their low-pressure turbine (LPT) blades heralded the fruition of long-term TiAl development after more than forty years of extensive research [4]. A consensus was reached twenty years ago that these intermetallic systems must have a refined fully lamellar microstructures to offer the best balance of properties [5]. Boron has been introduced to refine lamellar colonies to 50 - 300 μm without costly post-casting thermal processing [6], with the refined alloys having significantly improved room temperature ductility to a level of about 1% without degrading the creep resistance [7]. One of the first refined alloys with boron addition is Ti45Al2Mn2Nb1B (Ti45221B) which was developed around 1990 [7], with boron continuing to be used to refine the grain size in the latest wrought beta-solidifying TNM alloys [8]. It has established itself as an almost indispensable

* Corresponding author at: Institute of Structural Materials, Swansea University, College of Engineering, Fabian Way, Crymlyn Burrows, Swansea University Bay Campus, Swansea SA1 8EN, UK.
E-mail address: jing.li@swansea.ac.uk (J. Li).

https://doi.org/10.1016/j.matdes.2020.109064

alloying element to cast TiAl alloys with various compositions, working with multiple boron sources e.g. aluminium and tantalum boride, provided the molten pool is maintained long enough to fully dissolve borides and boron distribution is homogenised in the liquid [9].

It has been proven that large-sized borides are detrimental to ductility, and can reduce ductility to near zero [10]. More novel systems have resulted in the inclusion of more or new refractory elements, such as Nb, Hf, Ta, Mo and W, which may improve oxidation/corrosion and creep resistance, thus improving the overall temperature capability of alloys. However, the alloying modification will inevitably affect the boride size and morphologies which are closely related to the alloying element species and the solidification conditions [11]. Some of strong boride formers e.g. Ta and Nb, may interact with borides during their formation and alter their solidification behaviour [9]. This implies that if the boride formation behaviour is not properly understood, resulting in unoptimised solidification processes, modified alloys may be rendered practically useless.

A range of stoichiometries and crystal structures of the borides in TiAl alloys have been reported. There are four types of titanium borides found in TiAl alloys: TiB_2, Ti_3B_4, TiB (B27) and TiB (B_f) [9], which acquire different morphologies depending on the referred crystal growth directions of that particular phase. The most common structure of monoborides is orthorhombic TiB(B27) which has different morphologies. Extensive information on TiB (B27) size and morphology have been accumulated in recent years. The two most often observed TiB (B27) are plank-like and flake-like (curvy) morphologies which may grow to 200–300 μm in length, ~1 μm in thickness and ~10 μm in width [9]. The broad surface of plank-like TiB (B27), formed during solidification under slow and medium cooling conditions, is (100)B27 [12]. The quickest growth direction is [010]B27 [12]. De Graef et al. [13] observed irregular plate-like, as well as needle-shaped precipitates consisting of mixed TiB with the B27 and B_f structures in β-solidified TiAl alloy. Ribbon-like borides are common in low Al, high alloyed systems or alloys containing Ta, W or high Nb. Kartavykh et al. [14] found that in high Nb containing TiAl alloys the prevailing boride form was B27. It composed of many thin plates or flakes lying parallel to the ribbon plane. The ribbons are comprised mainly of the B_f monoboride and metallic B2 phases, which adopt orientation relationship (OR): [001] B_f // [001] B2; with (010)B_f // (010)B2 [15].

The information on the size and morphology of TiB (B_f) precipitates is very limited. Compared to TiB (B27), TiB (B_f) is less common, with no published systematic study on TiB (B_f) morphologies. It is known that B_f structure is metastable phase relative to the other three types of titanium boride in the Ti-Al-B ternary, however, it is a stable phase in Ti-Al-B-X quaternary and higher order alloys (where X = Nb, Ta and/or Zr) [15]. TiB (B_f) was found in Ti44Al4Nb4Zr1B 1 kg button ingots and also Ti44Al8Nb0.1B 20 g finger ingots, related to fast cooling during solidification [15,16]. The understanding of the alloy species-cooling condition-formation of flake TiB-mechanical property relationship has been far from satisfactory. However, investigation is still required as to the formation of flake TiB and its effect on ductility and whether the formation of flake TiB is affected by alloying or solidification condition. The current work focuses on systematically investigating the boride formation behaviour, especially the flake-like curvy boride in TiAl alloys with different alloying modifications and different cooling rates. The crystal structure of curvy flake borides and their effect on mechanical properties are also investigated.

2. Experimental

2.1. Raw material and processing

2.1.1. As-cast variants of Ti45Al2Mn2Nb1B button

Various cast Ti45221B variants of composition listed in Table 1 were measured by energy-dispersive x-ray spectroscopy (EDS) and were prepared via cold hearth plasma arc melting in the form of 1 kg ingots.

Table 1
Variants of as-cast Ti45221B with alloy composition.

Alloy composition (at. %)	Analysis
Ti-45Al-2Mn-2Nb-0.8B(Ti45220.8B)	Effect of Al
Ti-48Al-2Mn-2Nb-1B(Ti48221B)	
Ti-50Al-2Mn-2Nb-1B(Ti50221B)	
Ti-45Al-2Mn-2Nb-0.8B	Effect of Nb
Ti-45Al-2Mn-4Nb-0.8B*	
Ti-45Al-2Nb-2Hf-0.8B*	Effect of Hf
Ti-44Al-4Nb-4Hf-1B	
Ti-45Al-2Cr-2Hf-0.8B	
Ti-45Al-2Mn-4Ta-0.8B*	Effect of Ta
Ti-45Al-2Nb-2Ta-0.8B	
Ti-46Al-8Nb-1B	Effect of high Nb content

* Samples used for TEM analysis.

Feedstock taken from ingots was melted into 20 g finger ingots using non-consuming arc remelting in a water-cooled copper crucible under an Argon atmosphere to ensure the same solidification conditions and improve homogeneity. Because the homogeneity of the 1 kg ingots has already been improved before arc remelting into 20 g buttons, the arc remelting was only repeated twice. A thin slice was taken from the middle of each finger ingot by electro-discharge machining (EDM), with scanning electron microscopy (SEM) samples prepared by conventional metallographic grinding and polishing procedures. All of the as-polished samples were chemically etched with Kroll's reagent of 2 vol% hydrogen fluoride (HF), 12 vol% nitric acid (HNO3) and balance water for 2 to 5 s.

Among these 20 g finger ingots, three ingots with typical composition were selected for investigating their crystal structures by transmission electron microscopy (TEM), which are Ti-45Al-2Nb-2Hf-0.8B, Ti-45Al-2Mn-4Ta-0.8B and Ti-45Al-2Mn-4Nb-0.8B. TEM samples were prepared by twin-jet electropolishing to perforation in a Struers Tenupol 3 apparatus using an electrolyte consisting of 5% of perchloric acid, 60% of Methanol and 35% of 1-Butanol at 243 K and 20 V/0.5–1 A. Liquid nitrogen was used to cool the electrolyte to the desired temperature.

2.1.2. Batches of Ti-45Al-(4-6) (X, Y)-1B

To compliment the as-cast variants, batches of Ti-45Al-(4-6) (X, Y)-1B, where X, Y═Cr, Mn, Nb and Hf were prepared for room temperature tensile testing. The actual chemical compositions were measured by EDS, with tensile properties from the tests given in Table 2. There were seven test pieces of Ti45Al2Mn4Nb1B (2Mn4Nb) in total, five of which were tested by the author and two tests of each variant were carried out by Rolls-Royce plc., for the tests not carried out by the author the stress-strain curves are unavailable. Tensile test pieces were prepared via cold hearth plasma arc melting in the form of 1 kg semi-spherical buttons. The buttons were subsequently HIPped at 1260 °C and 150 MPa for 4 h aiming to obtain a fully lamellar microstructure as well as removing the casting porosity. The oxygen content in the test bars was approximately 1000 wtppm. Importantly, all samples of the same composition were taken from the same arc melted ingot.

Table 2
Alloying composition and elongation tensile test results of batches of Ti-45Al-(4-6) (X, Y)-1B, where X, Y═Cr, Mn, Nb, Hf.

Alloys	2Cr2Nb		2Mn4Nb							2Nb2Hf	
Num. samples	1	2	1	2	3	4	5	6	7	1	2
El. (%)	0.5	1.5	0.3	0.6	0.9	1.1	1.2	1.3	1.3	0.1	0.35
YS (MPa)	518	489	529	508	515	539	532	520	489	–	582
UTS (MPa)	590	682	550	599	670	680	695	700	664	572	634

2.2. Microstructural characterisation

A JEOL 7000 field-emission gun SEM was used for collecting data on boride size and morphology in the Ti45221B variants with different alloying species and solidification conditions. Both secondary electron and backscattered mode were used for microstructural characterisation at an accelerating voltage of 20 kV. The 20 g-finger ingots cooled down rapidly during solidification owing to their small volume. A temperature drop of 600 °C after 1 min from power off was noted, thus the cooling rate during solidification was estimated to be in the order of $1°Cs^{-1}$ considering the fact that cooling rate is most rapid at high temperatures during the initial stages and drops over time. Observations were made in areas along the white solid line, as shown in Fig. 1. The regions near the shrinkage have relatively faster cooling rates than the middle regions away from the surface and the regions in contact with the copper crucible have the fastest cooling rate, due to changes in thermal gradient. The white dotted line shows the boundary between the first and second melting stage. EDS analysis on TEM samples was carried out on an Oxford Instruments FEI TECNAI (STEM) with Silicon Drift Detector (SDD) and field emission gun, with the TEM thin foil tilted at 15°.

2.3. Titanium boride crystal structure

TEM experiments were performed using a JEOL 2100 HT TEM operating at 200 kV. Bright-field (BF) imaging techniques were used to observe the morphology of precipitates. To identify crystal structure, at least three selected area diffraction (SAD) patterns were taken with different zone axes from the same boride precipitate. The tilt angles between those different zone axes were recorded and calculated. Kikuchi lines were used to help follow the tilting direction. Before taking SAD patterns on the zone axis of boride, the zone axis of gamma phase should be tilted to low index axis e.g. [100] and [101] and take a SAD pattern at this zone axis. This is in order to use gamma phase as a reference for calibration of the camera constant, thus allowing the d spacing of boride to be worked out according to the basic formula of electron diffraction: $L\lambda = Rd$.

2.4. Analysis of tensile testing

Tensile testing was carried out at room temperature on test pieces with a 12 mm gauge length and a diameter of 4 mm, with an initial strain rate of $1 \times 10^{-4}\ s^{-1}$. To assess the influence of flake boride on the tensile ductility in cast TiAl alloy, eight tensile test pieces post mechanical testing were cut into two parts by a Struers Accutom cutting machine. One half was used for microstructural characterisation, the other for fracture surface analysis.

3. Results

3.1. Microstructural evolution of boride

The effect of different alloying species and cooling rate on boride size and morphology was investigated in as-cast variants of Ti45221B buttons. The typical as-cast microstructures of Ti-(45, 48, 50) Al-2Mn-2Nb-(0.8-1) B are shown in Fig. 2. The fully lamellar microstructure was achieved in Ti45220.8B and Ti48221B. The ribbon-like particles with bright contrast are titanium boride precipitates, which are randomly distributed throughout the alloy matrix. Boride morphology in Ti45220.8B shows the typical response to the cooling rate; being thick and straight under slow cooling and changing to thin and curvy with increasing cooling rate. The boride morphology in Ti48221B's slow cooled area is not the same as in the corresponding area in Ti45220.8B, being curvy instead. A mixed microstructure of lamellar colonies and γ grains was found in Ti50221B, with boride in thin flake-like form, dark in contrast, manifesting itself as TiB_2. It seems that the morphology of TiB_2 in this alloy is not as sensitive to cooling rate as that of the boride in Ti45220.8B in the investigated cooling rate range. Bright ridges can only be observed in Ti45220.8B and Ti48221B, not in Ti50221B, which were formed during β to α phase transformation at a late stage when heavy β stabilising element Nb was expelled from the α laths into the remaining β. Fig. 3 shows as-cast microstructures of Ti-45Al-2Mn-4Nb-0.8B in which the Nb concentration was increased compared to Ti45220.8B. It appears that the increase in Nb by 2% did not change the trend of boride morphology against cooling rate significantly.

The as-cast microstructures of Ti-45Al-2Nb-2Hf-0.8B, Ti-44Al-4Nb-4Hf-1B and Ti-45Al-2Cr-2Hf-0.8B are shown in Fig. 4 to investigate the effect of Hf on microstructure. The contrast in the matrix is very strong, which resulted from microsegregation of Hf. Compared to boride in the TiAlMnNb alloys, boride precipitates in all the three Hf-containing alloys are thin flakes, with most of them slightly curvy. These curvy borides appeared not only in an area close to the chilling zone, but also distributed in the slow cooling area. Occasionally, thick straight boride ribbons were observed. The as-cast microstructure of the Ta-containing alloys, Ti-45Al-2Nb-2Ta-0.8B and Ti-45Al-2Mn-4Ta-0.8B are presented in Fig. 5. Compared to the boride formations in the previous alloys, those in the Ta-containing alloys have unique features. Boride precipitates have strong bright contrast in the BSE micrographs, they tend to be coarse and straight and to a lesser extent influenced by the cooling rate. Fine, thin and curvy boride precipitates are rare, especially in the 4Ta alloy. Additionally, the volume fraction of boride precipitates appears much higher than that in other alloys with the same boron concentration. The microstructure of a high Nb alloy, Ti-46Al-8Nb-1B, is shown in Fig. 6. Whilst the trend of boride morphology varying with the cooling rate is very similar to that in Ti45220.8B, the development of thin curvy borides at high cooling rates is more profound in the higher Nb alloy.

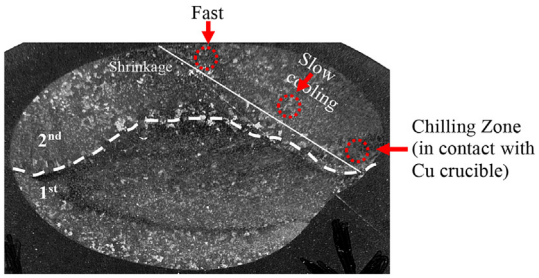

Fig. 1. Cross section area of the sliced 20 g finger ingot and the regions sampled.

3.2. Crystal structure of TiB

The crystal structures of boride precipitates, especially curvy flake borides observed in the as-cast buttons were determined. One alloy from each group of Hf-containing, Nb-containing and Ta-containing alloys are selected, whose chemical compositions are Ti-45Al-2Nb-2Hf-0.8B, Ti-45Al-2Mn-4Nb-0.8B and Ti-45Al-2Mn-4Ta-0.8B respectively. Curvy borides from each of the three typical compositions were selected for TEM characterisation and three selected area diffraction (SAD) patterns were tilted.

3.2.1. Ti-45Al-2Nb-2Hf-0.8B

Fig. 7 (a) shows the many beam Bright Field (BF) image of a typical curvy boride embedded in the Hf-containing microstructure showing the overall curvature of the flake. The red circle indicates where the SAD patterns were taken. Fig. 7 (b) to (d) is the corresponding SAD patterns from this precipitate in the zone axis of $[7\bar{1}2]$, $[3\bar{1}0]$ and $\left[3\bar{1}2\right]$, which has been identified as titanium monoboride (TiB) with an orthorhombic B_f structure. The lattice parameter is a = 0.323 nm, b = 0.856 nm, c = 0.305 nm. The thickness of the curvy boride observed here is about 300 nm. B2 structure at the zone axis of $\left[2\bar{1}0\right]$ was

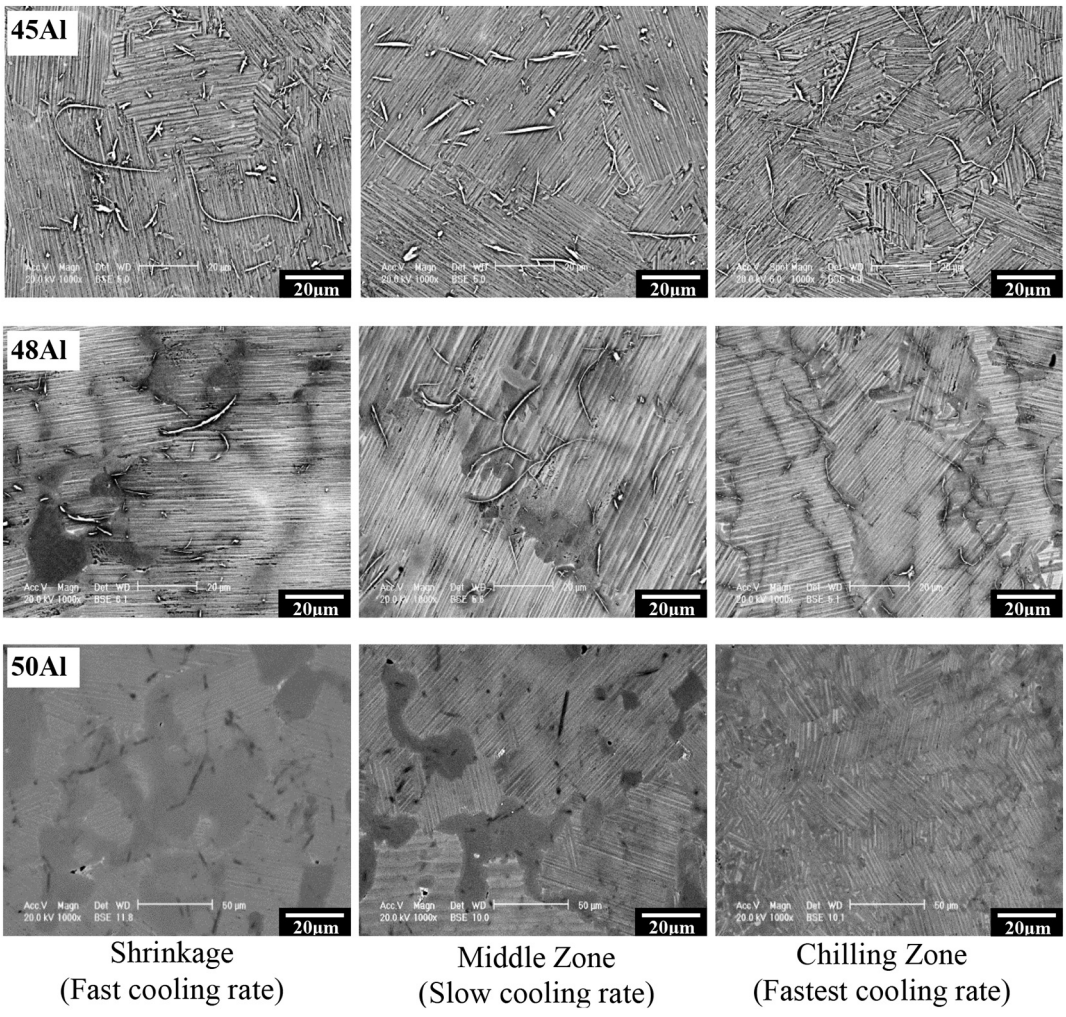

Fig. 2. BSE micrographs of Ti45Al-2Mn-2Nb-0.8B, Ti48Al-2Mn-2Nb-1B and Ti50Al-2Mn-2Nb-1B at the three indicated ingot regions.

found in the SAD pattern of B_f $[20\bar{1}]$, as shown in Fig. 8. Blue lines are for B_f structure whilst white lines are for B2 structure. There is no evidence of a well-defined orientation relationship between the borides and the surrounding metallic phases, therefore, the B2 phase must correspond to the embedded metallic layers. The OR between the B2 phase and the TiB (B_f) phase is found to be $[20\bar{1}]$ B_f // $[2\bar{1}0]$ B2.

3.2.2. Ti-45Al-2Mn-4Nb-0.8B

Fig. 9 (a) shows the morphology of curvy borides in the Nb-containing microstructure, revealing less embedded laths inside the boride. This boride precipitate has TiB (B_f) structure judged from the SAD patterns in the zone axis of [514] and [101], as shown in Fig. 9 (b) to (c). The thickness of the curvy boride observed here is 100-300 nm on average, which is not significantly different from that found in Ti-45Al-2Nb-2Hf-0.8B.

3.2.3. Ti-45Al-2Mn-4Ta-0.8B

As previously shown, coarse and straight ribbon boride dominate whereas fine and curvy flake boride are rare in Ta-containing alloys. Fig. 10 (a) shows the many beam TEM image of a long “curvy” boride.

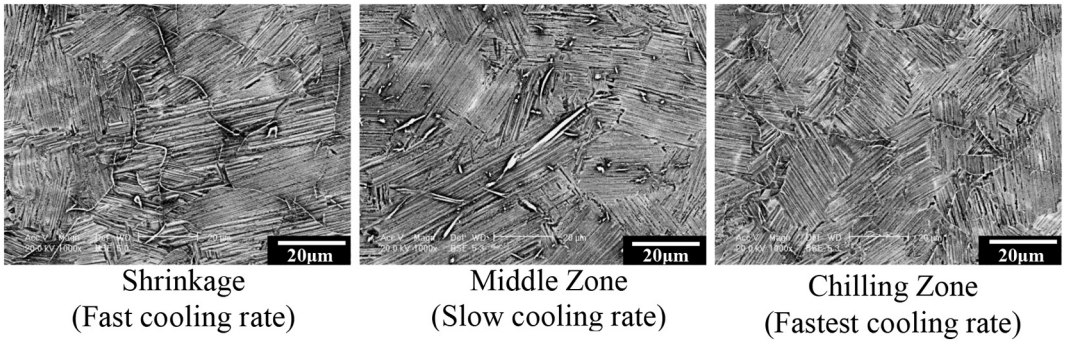

Fig. 3. BSE micrographs of Ti45Al-2Mn-4Nb-0.8B.

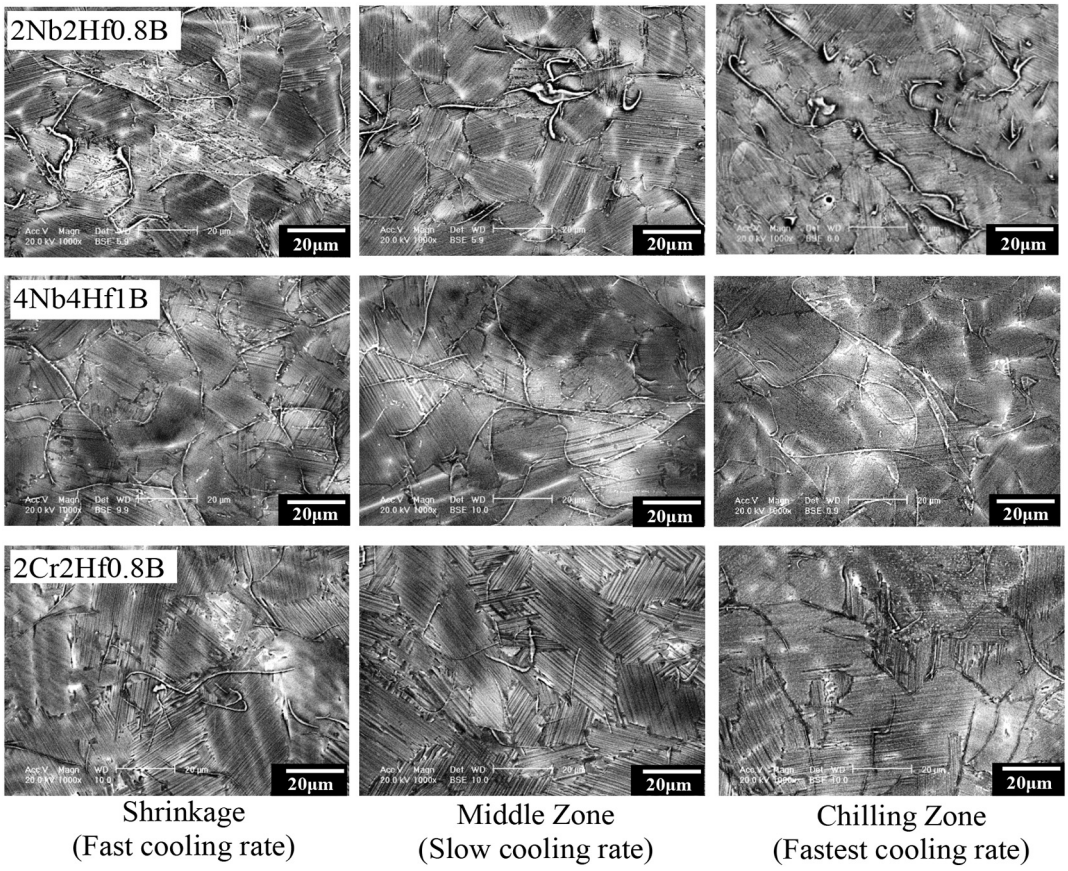

Fig. 4. BSE micrographs of Ti-45Al-2Nb-2Hf-0.8B, Ti-44Al-4Nb-4Hf-1B and Ti-45Al-2Cr-2Hf-0.8B.

It is worth noting that this curvy boride is actually composed of several boride segments, each of which is straight and has lots of ledges. This "fake" curvy boride has TiB (B27) structure, judged from the SAD patterns as shown in Fig. 10 (b) to (d).

Fig. 11 (a) shows the TEM image of the curvy boride morphology, which is different from that in Fig. 10, with the curvature of this boride being continuous. Fig. 11 (b) to (d) are the corresponding SAD patterns from this boride in the zone axis of [310], [110] and [211], which confirm that it has TiB (B_f) structure. It should be noted that although these borides have a curvy shape, it is generally thicker and wider than that of in the other two alloys, especially thicker than the Hf-containing alloy.

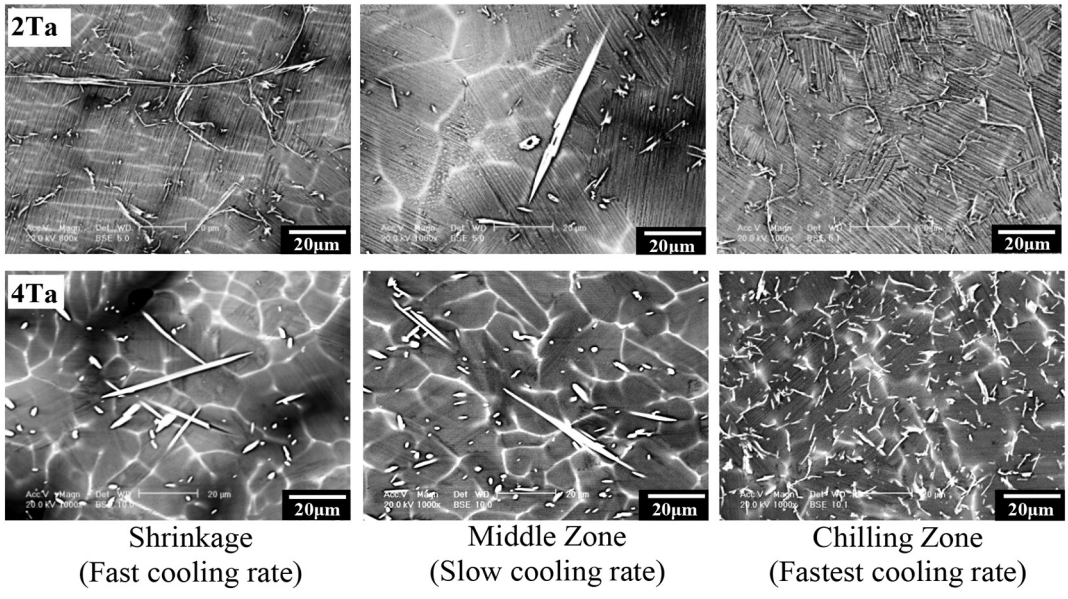

Fig. 5. BSE micrographs of Ti-45Al-2Nb-2Ta-0.8B and Ti-45Al-2Mn-4Ta-0.8B.

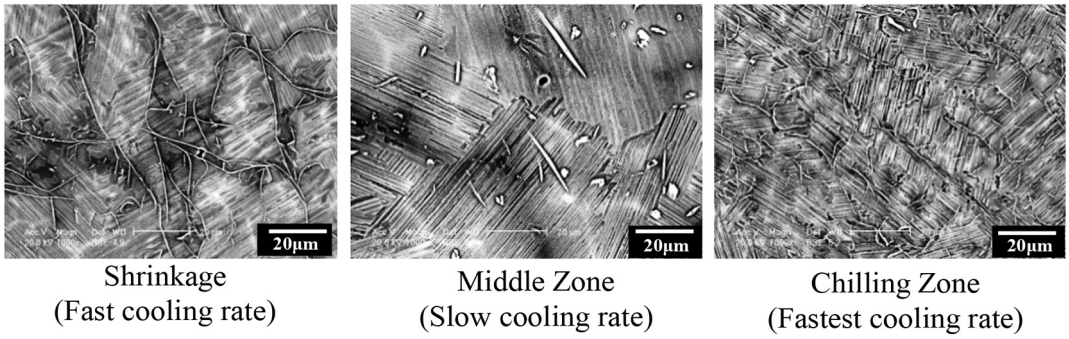

Fig. 6. BSE micrographs of Ti-46Al-8Nb-1B.

3.3. Compositional analysis

EDS analysis on the titanium borides and matrix material of the TEM foils is summarised in Table 3, showing that all titanium boride particles contain some alloying elements. Alloying elements Nb and Ta have concentrations in borides higher than those in the matrix, where as Hf and Mn, have concentrations in boride lower than those in the matrix. The Ta is partitioned to the greatest extent to the borides with ratios between 11.6 and 29.2. The Nb concentration in TiB is always higher than that in the matrix varying from 1.7 to 2.3. The Hf concentration in TiB is shown to be 1.6 which is lower than that in the matrix. The above observations are consistent with Liu et al. [17] who reported that TiB particles are enriched with Nb and Ta, but depleted with Mn.

3.4. Effect of flake curvy boride on tensile ductility

Small grain size is not always accompanied by high ductility in boron-containing TiAl alloys, since it has been proven that large-sized straight-shaped TiB is detrimental to tensile ductility [10,18]. However, the effect of flake-like curvy boride on ductility remains unknown. Microstructural characterisation and fracture surface analysis was carried out on tensile test pieces as listed in Table 2. These alloys are divided into three groups (1) Ti45Al2Mn4Nb1B (2Mn4Nb); (2) Ti45Al2Cr2Nb1B (2Cr2Nb); and (3) Ti45Al2Nb2Hf1B (2Nb2Hf). There are seven tensile test pieces in 2Mn4Nb group with El. = 0.3%, 0.6%, 1.0%, 1.1%, 1.2%, 1.3% and 1.3%, the lowest and highest ductility (0.3% and 1.3%) have been selected for further analysis. The stress strain curves of the five tensile test pieces of 2Mn4Nb are shown in Fig. 12. Minimal difference in lamellar colony size is found, which can be as small as 20 μm, in comparing the microstructures of all tensile test pieces.

Boride morphologies and fracture surfaces of 2Mn4Nb with 0.3% El. are shown in Figs. 13(a) and 14 (a). Curvy fine TiB dominates whereas straight thick boride are rarely observed. Curvy but coarse facets can be found throughout the fracture surface, which is the failed interfaces of TiB, most of them are about 100-200 μm long, equivalent or larger than the average lamellar colony size. Boride morphologies and fracture surfaces of 2Mn4Nb with 1.3% El. are shown in Figs. 13(b) and 14(b), which differs significantly to the 0.3% El test piece, straight boride facets now dominate and the curvy facets are rare. It seems the facet surface in the high ductility test piece is smoother than that of the low ductility test piece. The length of the board facet is about 250 μm, which is double the length of the curvy facets. This implies that large long borides are not always detrimental to ductility.

Figs. 13 (c-d) and 14 (c-d) show the boride morphology and fracture surface of 2Cr2Nb with 0.5% El and 1.5% El. The situation of 2Cr2Nb is the same as 2Mn4Nb, with the ductility of samples with large area fractions of thin curvy boride never higher than 1% El. Hf containing alloy 2Nb2Hf has the lowest ductility among all the tensile test pieces, 0.1% and 0.35%. According to the results from the microstructural characterisation of as-cast samples, Hf promotes the formation of curvy borides, regardless

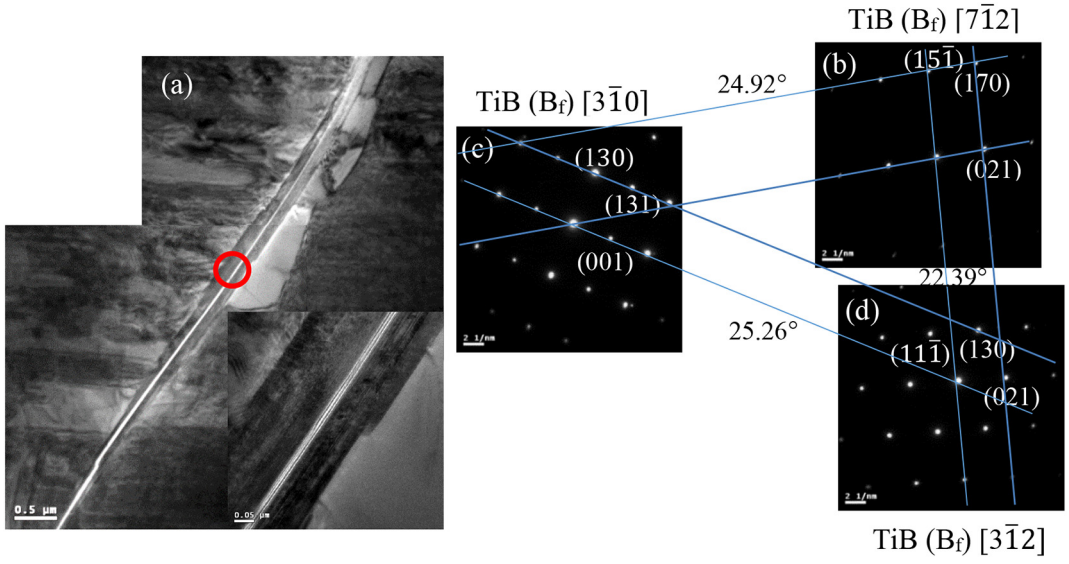

Fig. 7. TEM images of Ti-45Al-2Nb-2Hf-0.8B (a) morphology of boride; SAD patterns of in the TiB (B_f) zone axis (b) [7$\bar{1}$2], (c) [3$\bar{1}$0] and (d) [3$\bar{1}$2]. The tilting angles between (b) and (c), (c) and (d) and (b) and (d) are 24.92°, 25.26° and 22.39°, respectively.

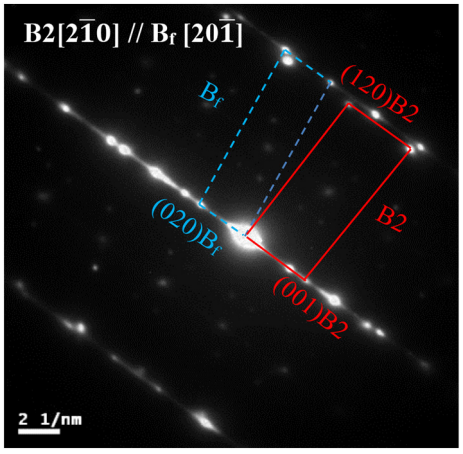

Fig. 8. SAD pattern in TiB (B_f) showing B2 structure at zone axis of $[2\bar{1}0]$.

of cooling rate, resulting in large area fractions of curvy boride formations. Boride morphology and fracture surface of 2Nb2Hf with 0.1% El and 0.35% El are shown in Figs. 13 (e-f) and 14 (e-f), showing the same character as the other two alloy groups with lower ductility and curvy borides can be found on both the microstructure and fracture surface.

4. Discussion

The effect of alloying elements and cooling rate on boride size and morphology of the ten as-cast finger ingots have been quantitatively investigated. The effect of Al on the boride morphology was investigated in Ti-(45, 48, 50)Al-2Mn-2Nb-(0.8-1)B according to different cooling conditions. Boride morphology in Ti50221B are in the form of thin flakes and dark contrast whilst Ti45220.8B and Ti48221B have ribbon-like boride morphology with bright contrast, regardless of cooling rate. Increasing the Al concentration in the Ti-Al-B system could change the structure of primary borides from TiB to Ti_3B_4 and finally to TiB_2 according to the schematic Ti-Al-B liquidus projection [13,19]. When the Al content is more than 45 at. %, TiB_2 is the only possible boride type formed. However, when 2 at. % of monoboride former Nb is added to the alloy, TiB monoborides can be stabilized to the higher 48 at. % Al content. The result of these three alloys matches the binary TiAl solidification pathway where low alloying elements would not cause a large shift of phase boundaries. The full lamellar microstructure was achieved in Ti45220.8B and Ti48221B whereas a mixed microstructure of lamellar colonies and γ grains was found in Ti50221B, because the level of Al content affects the volume fraction of the β phase which decreases with increasing Al concentration. Alloys with 49% Al or higher solidify through the α phase as the β phase is more effective in rejecting boron into the liquid than the α phase. Alloys with a large volume fraction of solidifying β phase would be able to build up boron-enriched liquid fronts more quickly, leading to increased efficacy of grain refinement.

Increased cooling rates could delay the onset of boride precipitation and cause boride precipitates segregate to interdendritic regions. Curvy flake borides are primarly located at the interdendritic regions where cooling rate is rapid, indicating that boride formation occurred after the β dendrites were formed, likely at a stage when the β dendrites growth was almost to its end. Conversely, when cooling rate is low, coarse and straight boride precipitates are found to be distributed randomly throughout the alloy matrix embedded within the β dendrites, with some parallel to the stems of the dendrites. This indicates that those borides have co-grown with the β dendrites or were only slightly later than the leading β phase during solidification.

Hf and Ta partitioning behaviour in boride was investigated by microstructural and compositional characterisation. The microstructural results indicate that Hf promotes formation of thin curvy boride flakes, whereas Ta promotes formation of thick straight boride ribbons in the studied cooling rate range, regardless of the alloy composition. One of the most significant differences in boride morphologies is that borides are thicker and show stronger bright contrast in Ta-containing alloys when compared with Hf-containing alloys, whether curvy or straight in morphology. According to the compositional analysis, Ta is a strong boride-former and high concentrations in TiB has significant effects on microstructures and grain refinement. The stable TiB borides are formed at 45 at.% Al in the studied alloys, which can strongly segregate into

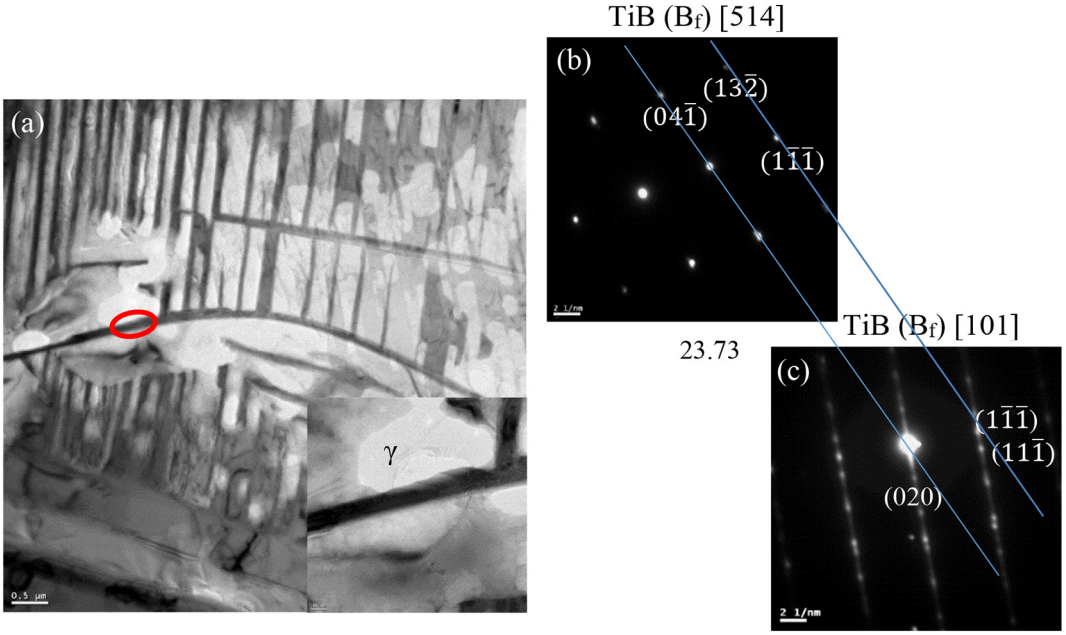

Fig. 9. TEM images of Ti-45Al-2Mn-4Nb-0.8B (a) morphology of boride; SAD patterns in the TiB (B_f) zone axis (b) [514] and (c) [101]; the tilting angles between (b) and (c) is 23.73°.

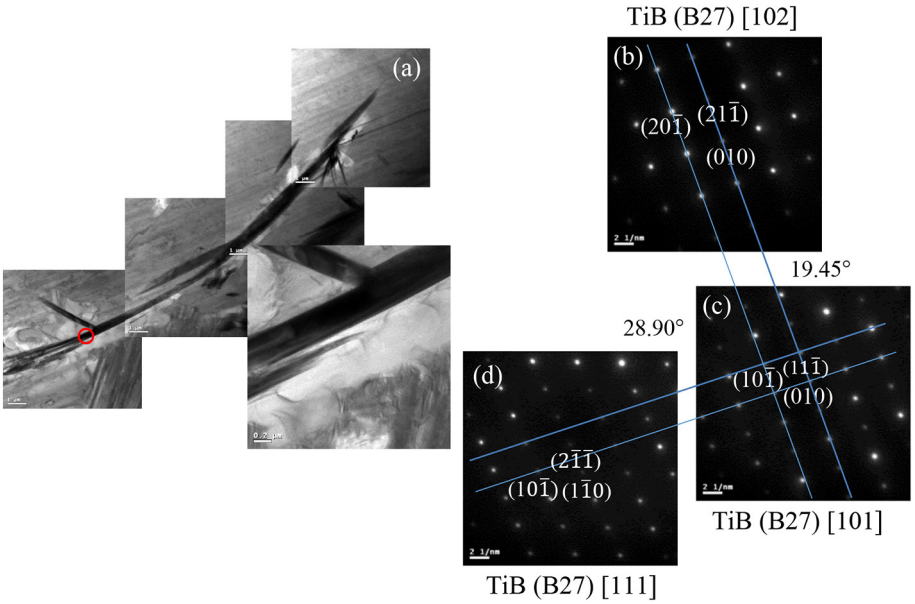

Fig. 10. TEM images of Ti-45Al-2Mn-4Ta-0.8B: (a) boride morphology; SAD patterns in the TiB(B27) zone axis (b) [102], (c) [101] and (d) [111]. The tilting angles between (b) and (c), (c) and (d) are 19.45° and 28.90°.

boride forming (Ti, Ta)B. Hf is also a boride former (HfB and HfB_2) but to a lesser extent. These observations extend the results of Hu [20] and Larson et al. [21] who reported the formation of TiB in at least 47 at.% Al alloys. According to the grain refinement mechanism, alloying additions such as Ta and Nb that are strong boride formers will reduce the boron concentration in the liquid and reduce the effectiveness of the boron as a grain refiner.

A major concern in the casting of TiAl alloys is the growth direction of titanium borides in the molten metals and it is this anisotropic growth that shapes the morphology of boride precipitates [9]. The crystal structure of boride was identified by TEM in the as-cast Hf, Nb and Ta-containing alloys, with results confirming that curvy thin flake boride has TiB(B_f) structure and has high aspect ratios with a (010) habit plane and fastest growth direction along [001]. The (001) planes are stoichiometric and thus growth of a B_f particle along [001] requires only very short-range atomic re-arrangements and (100)B_f planes probably grow faster than growth normal to the (010)B_f planes, thus giving rise to the elongated morphology of the B_f crystals with habit planes at 70° from the [100]B27 facets, these are shown on sample surfaces as thin curvy lines owing to intersection effects. However, thick straight ribbon boride is identified in the form of TiB with B27 structure with the fastest growth direction along [010]. No matter which alloying element has been added into the alloy, whether Hf, Nb or even Ta, as long as curvy shaped boride flakes formed, the boride has TiB(B_f) structure. Fast cooling rates and the addition of Hf promote the formation of fine curvy flake boride which form preferentially with TiB(B_f) structure

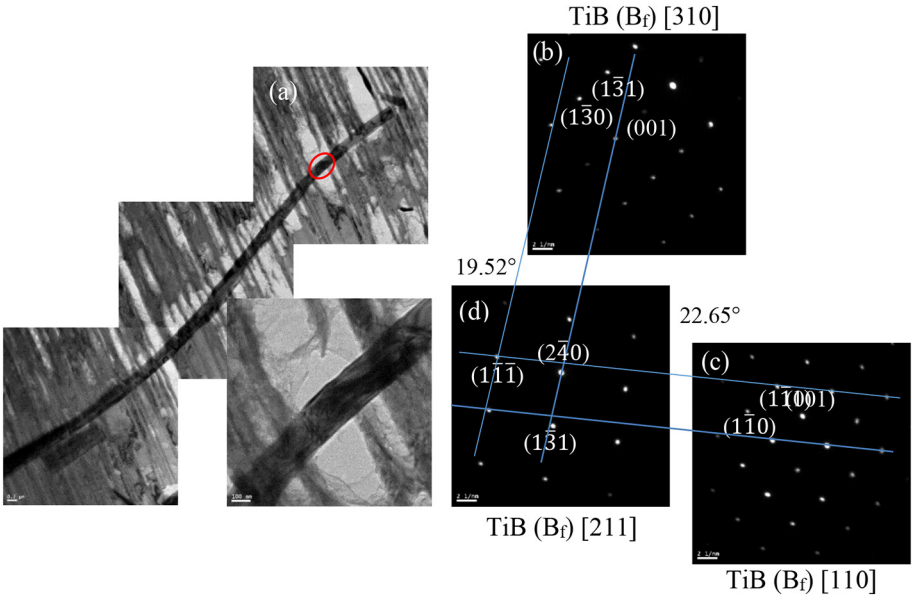

Fig. 11. TEM images of Ti-45Al-2Mn-4Ta-0.8B: (a) the morphology of boride. The red circle indicates where SAD patterns were taken; (b-d) the SAD pattern in TiB (B_f) zone axis (b) [310], (c) [110] and (d) [211]. The tilting angles between (b) and (d), (d) and (c) are 19.52° and 22.65°. (For interpretation of the references to colour in this figure legend, the reader is referred to the web version of this article.)

Table 3
The concentration of selected elements in matrix and titanium boride of the TEM samples.

Alloy		Concentration ratio			
		Nb	Hf	Ta	Mn
Ti-45Al-2Nb-2Hf-0.8B	Matrix	1.5	1.9		
	Boride	1.7	1.6		
Ti-45Al-2Nb-2Ta-0.8B	Matrix	1.5		1.7	
	Boride	2.3		11.6	
Ti-45Al-2Mn-4Ta-0.8B	Matrix			4.2	1.5
	Boride			29.2	0.1

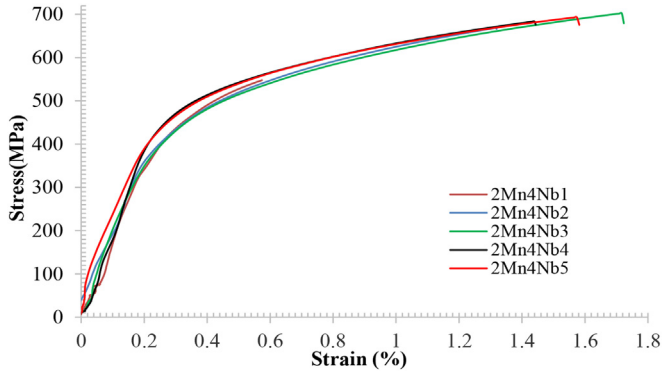

Fig. 12. Stress-strain response curves of 2Mn4Nb(1-5) samples.

rather than TiB(B27) structure. The boride formation mechanism for ribbon boride has been proposed by Hyman et al. [19], De Graef et al. [13] and Kitkamthorn et al. [15] for β and α solidified alloys, reporting that boride could either start as primary particles in the liquid or have co-grown with primary β dendrite. According to the ternary liquidus projection for alloys with 45 at. % of Al, assuming alloy with super-critical boron levels, borides form a eutectic mixture in the liquid ahead of the solidification front through the eutectic reaction:

$$L \rightarrow \beta + TiB \quad (1)$$

Once the solidification path reaches the monovariant line, boride will nucleate and grow concurrently with β-(Ti). Such borides are likely to have spent some time and have space to grow freely in the melt before they were trapped and constrained their growth by the matrix.

In order to understand the formation behaviour of curvy flake boride, it is of utmost importance to have a clear understanding of the relationship between the B_f and B27 monoboride structures. Liu et al. [17] reported that B_f and B27 structures have similar formation energy by performing first-principle calculations to compare the enthalpies of formation of the two TiB structures, in agreement with the calculation reported by De Graef et al. [13]. The lattice stabilities of these two structures are quite similar and the B_f structure is only slightly metastable relative to the B27 form. Similarly, Nandwana et al. [22] reported that the B_f and B27 structures have a fully coherent interface and low energy barrier for shearing of the B27 TiB to form B_f structure easily. B_f structure arises in response to a change in the melt chemistry and growth of the B_f phase is kinetically easier than that of the stable TiB_2 or Ti_3B_4 phases (which require more B to form) [13]. B_f phase has an excellent opportunity for nucleating on the B27 in the manner of repeated rotational twinning. Single B_f monolayer or two monolayers sandwiched between B27, exhibit the OR: $[001]B_f//[010]B27$; with $\{110\}B_f//(100)B27$ [15,22].

The above evidence suggests that at large undercooling, the fine curvy flakes are precipitated as secondary boride particles rather than by precipitation from a supersaturated solid solution, which will nucleate and grow epitaxially on pre-existing B27. Therefore, B_f structure is formed owing to its closer orientation relationship with the existing B27 phase, which favours nucleation on the (100) B27 planes, as well as its lower requirements for boron which facilitates growth from a melt dilute in this element. Curvy flake borides were mainly formed in the interdendritic liquid and when cooling rate is rapid. Borides are readily available at the interdendritic area during solidification because of the extremely low solubility of boride in solid (either β or α), therefore, they were expelled by solid into the interdendritic area. Borides precipitating at the end of solidification had no space and time to grow. Subsequently, the flakes grew coupled with the matrix and be constrained by the neighbouring matrix as they grow concurrently at the interdendritic region. They are then distorted by the physical force induced by the growth of the neighbouring matrix through the last

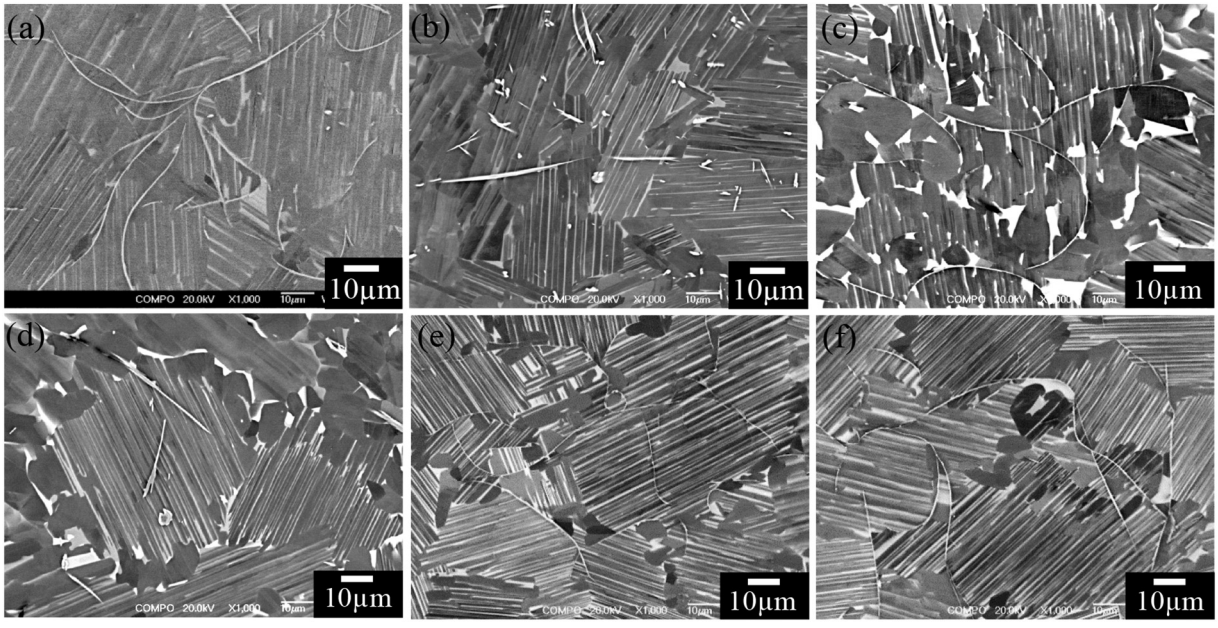

Fig. 13. Boride morphology of 2Mn4Nb with (a) 0.3% El. and (b) 1.3% El; 2Cr2Nb with (c) 0.5% El and (d) 1.5% El.; 2Nb2Hf with (e) 0.1% El. and (f) 0.35% El.

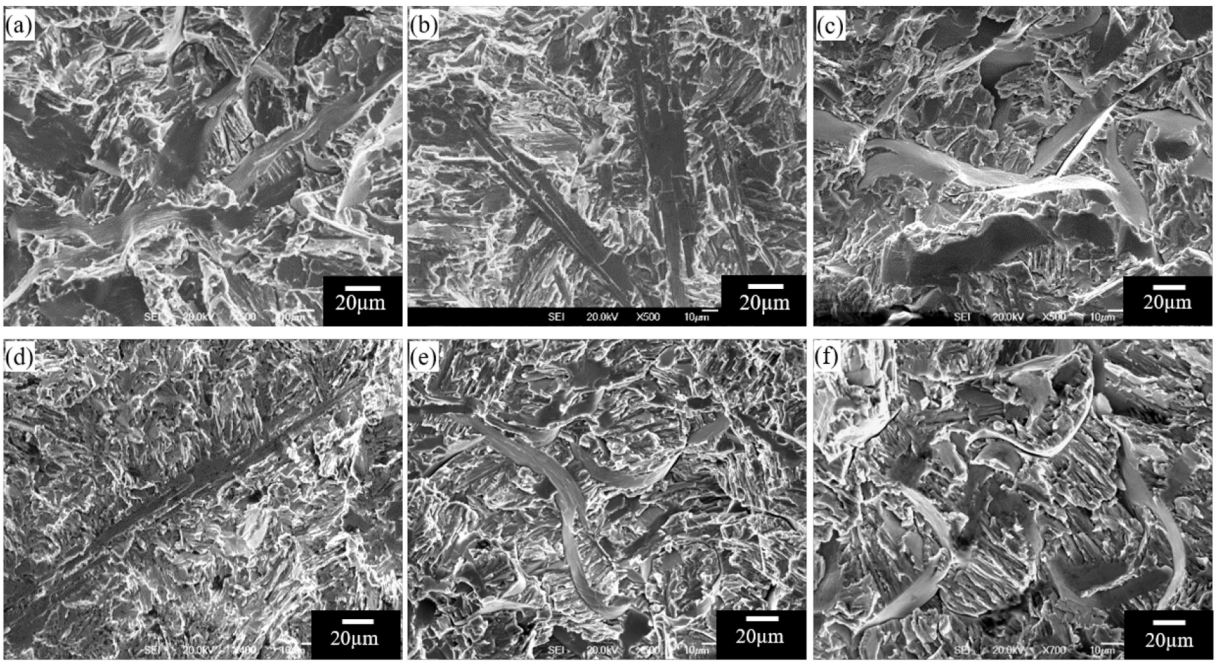

Fig. 14. Fracture surface of 2Mn4Nb1B with (a) 0.3% El. and (b) 1.3% El; 2Cr2Nb1B with (c) 0.5% El and (d) 1.5% El.; 2Nb2Hf1B with (e) 0.1% El. and (f) 0.35% El.

stages of solidification, leading to the boride shape being curved. The TEM crystallographic analysis indicates that curvy borides are a single crystal, which should not have bent crystal planes, so the curvature of these flakes could only be formed through stepwise fashion change on the atomic planes to give the overall morphology observed on a larger scale. In literature, Kitkamthorn et al. [15] have observed an unusual curvy shaped "ribbon" boride in a Ti-44Al-4Nb-4Zr-1B alloy and similar mechanism has been proposed. Contrarily, ribbon borides formed at the very beginning of solidification have enough space and time to grow into coarse thick ribbons without being broken off. Those ribbons which have co-grown with β dendrite have already grown into coarse thick boride before they were constrained by the neighbouring matrix, therefore, their shape can no longer be altered.

As shown in Fig. 6, the development of thin curvy borides at high cooling rates is more profound in the higher Nb alloy. There are a number of reasons to account for this: (1) the formation of the B2 phase is a condition of the ribbon boride and high content of Nb is known to promote B2 ordering of the β phase [13,15]; (2) at high cooling rate, boride expelled into the interdendritic area and are precipitated as secondary boride particles with B_f structure, which will nucleate and grow epitaxially on pre-existing B27; (3) Nb has no time to be enriched in the β dendrites at high cooling rate and the high Nb content in the interdendritic regions creates a favourable condition to exceed the enthalpy minimum for the formation of the B27 structure of borides; (4) Hecht et al. [23] reported that Nb addition to boron containing TiAl alloys contributes to the stabilisation of the metastable *oC8* (B_f) structure of TiB against the stable *oP8* (B27) structure. They have also found the borides in a niobium-rich TiAl-based alloys has B_f structure. Therefore, it can be inferred that high cooling rate together with high content of Nb promote the formation of B_f structure.

The scatter of the room temperature ductility measured in the same arc melted ingot is quite large. It should be noted that arc remelting and instability of the atmosphere may contribute to inhomogeneous microstructure. Curvy borides were found both on fracture surfaces and microstructures in tensile test pieces with low tensile ductility, particularly in the Hf-containing specimens. The area fraction of curvy shaped facets in an alloy with low ductility is significantly higher than in the results showing a higher ductility, although it difficult to carry out quantitative analysis. This observation indicates that curvy boride has the strongest effect in reducing ductility regardless of alloy composition, therefore, it is of great importance to the determine the processing windows that avoid the formation of curvy boride. Improved tensile ductility is expected in Hf free alloys because curvy boride would not become the prevailing boride formation with appropriate cooling conditions. Curvy flake boride causes premature failure through promoting crack propagation via debonding between boride-matrix interfaces with cracking along the interfaces uninterrupted until the end of the boride precipitates. Thus, helping damage pass through neighbouring colonies in unfavourable orientations, leading to long cracks in alloys with small lamellar colonies. Therefore, it is of great importance control the size of boride precipitates during solidification and it is at least as critical as the lamellar colony size in improving room temperature tensile ductility.

5. Conclusions

The following can be concluded regarding the boride formation behaviour in TiAl alloys:

- Alloying elements and cooling rate are found to influence the boride size and morphology although their efficacy is different. Hf promotes the formation of thin curvy boride flakes whilst Ta promotes the formation of thick straight boride ribbons in the studied cooling rate range, regardless of alloy composition.
- Increasing the cooling rate during solidification means that the morphology of borides will change from thick straight ribbons to thin curvy boride flakes.
- The crystal structures of curvy borides are TiB with B_f structure, independent of alloying composition.
- Curvy borides are constrained by the neighbouring matrix as they grow concurrently at the interdendritic region and distorted by the physical force induced by the growth of the neighbouring matrix at the last stages of the solidification.

- Curvy borides have the strongest effect in reducing ductility, regardless of alloy composition. The ductility in Hf-containing alloy, which was found to promote curvy boride formation, was no more than 0.4%.

Data availability

The raw/processed data required to reproduce these findings cannot be shared at this time as the data also forms part of an ongoing study.

Declaration of Competing Interest

The authors declare that they have no known competing financial interests or personal relationships that could have appeared to influence the work reported in this paper.

Acknowledgements

The research was funded by the EPSRC Rolls-Royce Strategic Partnership in Structural Metallic Systems for Gas Turbines (grants EP/H500383/1 and EP/H022309/1). The provision of materials and technical support from Rolls-Royce plc is gratefully acknowledged. TEM work was performed at the University of Birmingham. The author would like to thank Dr. Dawei Hu for his supervision on this study.

References

[1] Y.-W. Kim, S.-L. Kim, Advances in gammalloy materials–processes–application technology: successes, dilemmas, and future, JOM 70 (4) (2018) 553–560.
[2] H. Fang, R. Chen, Y. Liu, Y. Tan, Y. Su, H. Ding, J. Guo, Effects of niobium on phase composition and improving mechanical properties in TiAl alloy reinforced by Ti2AlC, Intermetallics 115 (2019) 106630.
[3] S. Gong, Y. Shang, J. Zhang, X. Guo, J. Lin, X. Zhao, Application and research of typical intermetallics-based high temperature structural materials in China, Jinshu Xuebao/Acta Metallurgica Sinica 55 (9) (2019) 1067–1076.
[4] B. Liu, J. Li, D. Hu, Solidification and grain refinement in Ti(48–50)Al2Mn2Nb1B alloys, Intermetallics 101 (2018) 99–107.
[5] Y.-W. Kim, Ordered intermetallic alloys, part III: gamma titanium aluminides, JOM 46 (7) (1994) 30–39.
[6] D.E. Larsen, S. Kampe, L. Christodoulou, Effect of XD^{TM} TiB2 volume fraction on the microstructure of a cast near-gamma titanium aluminide alloy, MRS Proc. 194 (1990) 285.
[7] D.E. Larsen, L. Christodoulou, S.L. Kampe, R. Sadler, Investment-cast processing of XDTM near-γ titanium aluminides, Mater. Sci. Eng. A 144 (1) (1991) 45–49.
[8] H. Clemens, W. Wallgram, S. Kremmer, V. Güther, A. Otto, A. Bartels, Design of novel β-solidifying TiAl alloys with adjustable β/B2-phase fraction and excellent hot-workability, Adv. Eng. Mater. 10 (8) (2008) 707–713.
[9] D. Hu, Role of boron in TiAl alloy development: a review, Rare Metals 35 (1) (2016) 1–14.
[10] D. Hu, Effect of boron addition on tensile ductility in lamellar TiAl alloys, Intermetallics 10 (9) (2002) 851–858.
[11] M.E. Hyman, C. McCullough, C.G. Levi, R. Mehrabian, Evolution of boride morphologies in TIAL-b alloys, Metall. Trans. A 22 (7) (1991) 1647–1662.
[12] C.L. Chen, W. Lu, J.P. Lin, L.L. He, G.L. Chen, H.Q. Ye, Orientation relationship between TiB precipitate and γ-TiAl phase, Scr. Mater. 56 (6) (2007) 441–444.
[13] M. De Graef, J.P.A. Löfvander, C. McCullough, C.G. Levi, The evolution of metastable Bf borides in a Ti-Al-B alloy, Acta Metall. Mater. 40 (12) (1992) 3395–3406.
[14] A.V. Kartavykh, M.V. Gorshenkov, V.V. Tcherdyntsev, D.A. Podgorny, On the state of boride precipitates in grain refined TiAl-based alloys with high Nb content, J. Alloys Compd. 586 (2014) S153–S158.
[15] U. Kitkamthorn, L.C. Zhang, M. Aindow, The structure of ribbon borides in a Ti-44Al-4Nb-4Zr-1B alloy, Intermetallics 14 (7) (2006) 759–769.
[16] T.T. Cheng, The mechanism of grain refinement in TiAl alloys by boron addition — an alternative hypothesis, Intermetallics 8 (1) (2000) 29–37.
[17] B.G. Liu, L.H. Liu, W.D. Xing, R.C. Liu, R. Yang, P.A. Withey, J. Zhu, R. Yu, Structural stability and the alloying effect of TiB polymorphs in TiAl alloys, Intermetallics 90 (2017) 97–102.
[18] D. Hu, J.F. Mei, M. Wickins, R.A. Harding, Microstructure and tensile properties of investment cast Ti–46Al–8Nb–1B alloy, Scr. Mater. 47 (4) (2002) 273–278.
[19] M.E. Hyman, C. McCullough, C.G. Levi, R. Mehrabian, Evolution of boride morphologies in TiAl-B alloys, Metall. Trans. A. 22 (7) (1991) 1647–1662.
[20] D. Hu, Effect of composition on grain refinement in TiAl-based alloys, Intermetallics 9 (12) (2001) 1037–1043.
[21] D.J. Larson, C.T. Liu, M.K. Miller, The alloying effects of tantalum on the microstructure of an α2+γ titanium aluminide, Mater. Sci. Eng. A 270 (1) (1999) 1–8.
[22] P. Nandwana, N. Gupta, S.G. Srinivasan, R. Banerjee, A first principles study of commonly observed planar defects in Ti/TiB system, Comput. Mater. Sci. 150 (2018) 197–201.
[23] U. Hecht, V. Witusiewicz, A. Drevermann, J. Zollinger, Grain refinement by low boron additions in niobium-rich TiAl-based alloys, Intermetallics 16 (8) (2008) 969–978.